Dysregulation of Nrf2/Keap1 Redox Pathway in Diabetes Affects Multipotency of Stromal Cells

Piul S. Rabbani, Marc A. Soares, Sophia G. Hameedi, Rohini L. Kadle, Adnan Mubasher, Maria Kowzun, and Daniel J. Ceradini

Diabetes 2019;68:141–155 | https://doi.org/10.2337/db18-0232

The molecular and cellular level reaches of the metabolic dysregulations that characterize diabetes are yet to be fully discovered. As mechanisms underlying management of reactive oxygen species (ROS) gain interest as crucial factors in cell integrity, questions arise about the role of redox cues in the regulation and maintenance of bone marrow–derived multipotent stromal cells (BMSCs) that contribute to wound healing, particularly in diabetes. Through comparison of BMSCs from wild-type and diabetic mice, with a known redox and metabolic disorder, we found that the cytoprotective nuclear factor erythroid–related factor 2 (Nrf2)/kelch-like erythroid cell–derived protein 1 (Keap1) pathway is dysregulated and functionally insufficient in diabetic BMSCs (dBMSCs). Nrf2 is basally active, but in chronic ROS, we found irregular inhibition of Nrf2 by Keap1, altered metabolism, and limited BMSC multipotency. Forced upregulation of Nrf2-directed transcription, through knockdown of Keap1, restores redox homeostasis. Normalized Nrf2/Keap1 signaling restores multipotent cell properties in dBMSCs through Sox2 expression. These restored BMSCs can resume their role in regenerative tissue repair and promote healing of diabetic wounds. Knowledge of diabetes and hyperglycemia-induced deficits in BMSC regulation, and strategies to reverse them, offers translational promise. Our study establishes Nrf2/Keap1 as a cytoprotective pathway, as well as a metabolic rheostat, that affects cell maintenance and differentiation switches in BMSCs.

Addressing the clinical manifestations of type 2 diabetes and associated complications, such as chronic nonhealing wounds, necessitates a thorough understanding of pathological molecular and cellular events. Oxidative stress and flawed redox mechanisms induce metabolic deficiencies in diabetes and give rise to the characteristic of insulin resistance (1,2). An intriguing new direction of research, into the intersection of redox homeostasis and adult stem cell maintenance, raises questions about the effect of diabetes and hyperglycemia on stem/progenitor cells. Bone marrow–derived multipotent stromal cells (BMSCs) are known to participate in the wound healing process (3). The delay in tissue repair in diabetes that we have found (4,5) then raises the question of whether diabetic BMSCs (dBMSCs) are aberrant, or absent, or do not function in a regenerative environment. We aimed to explore whether diabetes and redox stresses critically affect BMSCs.

Metabolic changes and management of reactive oxygen species (ROS) are emerging as fundamental features that regulate cell identity across a range, from embryonic stem cells to induced pluripotent stem cells to bone marrow–derived hematopoietic stem cells (HSCs) and BMSCs (6,7). Studies on the metabolic regulation of HSC function and stemness are growing, but BMSC parallels are relatively scarce. Similar to their HSC neighbors (8,9), BMSCs thrive and remain multipotent in the hypoxic environment of the bone marrow (BM) (10). BMSCs also retain their capacity to differentiate along osteogenic, adipogenic, and chondrogenic lineages as they respond to nonnative sites with oxidative imbalance, such as a hypoxic wound (11). As metabolic and redox dysregulation are such central features of diabetes, the mechanisms that enable BMSC metabolic modulation and those that preserve cell integrity in oxidative imbalance may be compromised.

A pathway that encompasses metabolic and cytoprotective roles, and is disrupted in diabetes, is the nuclear

Hansjörg Wyss Department of Plastic Surgery, New York University School of Medicine, New York, NY

Corresponding author: Piul S. Rabbani, piul.rabbani@nyumc.org, or Daniel J. Ceradini, daniel.ceradini@nyumc.org

Received 28 February 2018 and accepted 9 October 2018

This article contains Supplementary Data online at http://diabetes.diabetesjournals.org/lookup/suppl/doi:10.2337/db18-0232/-/DC1.

factor erythroid–related factor 2 (Nrf2)/kelch-like erythroid cell–derived protein 1 (Keap1) pathway (12). Nrf2 is a transcription factor driving over 50 redox homeostasis–related genes and nearly 200 genes influencing metabolism and repair (13). Keap1 functions as an intracellular ROS sensor, as oxidants and electrophiles modify its cysteine residues. Without ROS, Keap1 binds to Nrf2 and promotes Nrf2 proteasomal degradation. ROS accumulation disrupts the Keap1-Nrf2 interaction. Nrf2 binds with small Maf proteins to antioxidant response elements in the regulatory regions of target genes. Key genes activated to respond to oxidative stress include NAD(P)H quinone oxidoreductase 1 (*NQO1*), manganese superoxide dismutase (*MnSOD*), heme oxygenase 1 (*HO-1*), glutamate cysteine ligase (*GCL*), and glutathione S-transferases (*GSTs*). A study found that human BMSCs in high ROS shift their metabolism to resemble differentiated cells and increase expression of antioxidant enzymes, MnSOD and catalase (14). Nrf2 overexpression can reduce ROS-induced apoptosis and cytotoxicity in BMSCs through upregulation of MnSOD and HO-1 (15). In diabetes and chronic hyperglycemia, unusually high levels of superoxide leak from the mitochondrial electron transport chain during aerobic respiration (2). The rate of ROS scavenging cannot compensate, resulting in damaging oxidation of cellular components (16). Previously, we found that despite high ROS, diabetic skin has low Nrf2 activation and subsequently has low antioxidant expression to affect delayed wound healing outcomes (5). Whether Nrf2/Keap1-mediated redox regulation plays a role in dBMSCs, or affects their identity, that in turn can influence BMSC response during diabetic wound healing is yet to be discovered. We postulate that to retain their multipotency and contribute to wound healing, BMSCs need to minimize ROS damage and preserve robust redox mechanisms.

Here, through comparison of wild type (WT) and dBMSCs, we identified dysregulated redox metabolism in dBMSCs leading to loss of multipotency, bias toward an adipogenic fate, and reduction of Nrf2-transcribed antioxidants. Using short interfering RNA (siRNA) against *Keap1*, we forced activation of the endogenous Nrf2 in dBMSCs to reprogram their metabolic and redox mechanisms, as well as restore multipotent cell behavior through Sox2 expression. Finally, we show that the Keap1 downregulation and Nrf2 activation–based rescue of dBMSCs enables them to participate in diabetic wound healing. We demonstrate the importance of intrinsic resistance mechanisms mediated by Nrf2/Keap1 in response to oxidative stress. Through the range of effects on redox homeostatic and metabolic maintenance mechanisms, the Nrf2/Keap1 pathway is critical in the maintenance of fate and function of adult BMSCs.

RESEARCH DESIGN AND METHODS

Mice

C57BL/6J and BKS.Cg-Dock7$^{m+/+}$Lepr$^{db/J}$ (blood glucose ≥400 mg/dL) strains were from The Jackson Laboratory. All protocols were approved by the Institutional Animal Care and Use Committee at New York University (NYU) School of Medicine.

BMSC Culture and Immunophenotyping

BM aspirates from 6–8-week-old mice were cultured in Mesencult at 37°C/5% CO_2/5% O_2. After the first media change, BMSCs were cultured in α-minimum essential medium supplemented with 15% FBS and 1% nonessential amino acids. Low-glucose and high-glucose medium contained 1 g/L and 4.5 g/L D-glucose, respectively. BMSCs were detached using 3:2 accutase:trypsin-EDTA, resuspended in 1× PBS/5% FBS/0.1% NaN_3, Fc blocked with anti-mouse CD21/CD23, stained with fluorophore-conjugated antibodies against CD45, Ter119, Sca1, PDGFRα, CD29, CD44, CD73, CD90.2, CD105, CD34, or flk1 (Miltenyi), and analyzed on a BD FACSCalibur and FlowJo.

Single-Cell Colony-Forming Assay

BMSCs were plated into 96-well plates at one cell per three wells. After 2 weeks, colonies stained with crystal violet were counted.

Adipogenic and Osteogenic Differentiation

For adipogenic induction, BMSCs were cultured in 0.5 μmol/L dexamethasone, 0.5 mmol/L IBMX, and 50 μmol/L indomethacin, with 1 mmol/L insulin for the initial 4 days, and analyzed at 14 days for Oil Red O–stained lipid droplets. For osteogenic induction, BMSCs were cultured in 100 nmol/L dexamethasone, 50 μmol/L ascorbate phosphate, and 10 mmol/L β-glycerophosphate, with 100 ng/mL bone morphogenetic protein 2 (BMP2) every 2 days. After 14 days, cells were analyzed for calcium deposits using alizarin red. Cells were photographed using a Zeiss Observer microscope.

Chondrogenic Differentiation

Cells (2.5×10^5) were pelleted in 15-mL tubes. Cell pellets were cultured in low-glucose α-minimum essential medium containing 1% FBS, 100 nmol/L dexamethasone, 50 μg/mL ascorbic acid 2-P, 40 μg/mL L-proline, 1% ITS/supplement B-D, and 1 mmol/L sodium pyruvate, with 10 ng/mL TGF-β3 and 100 ng/mL BMP2 added every 2 days. At 21 days, pellets were fixed, embedded in agarose, processed into paraffin blocks, sectioned, and stained for cartilage using Safranin O.

siRNA Transfection

BMSCs were seeded at 20,000 cells/cm^2. Dilutions of siRNA and Lipofectamine 2000 were mixed and incubated for 20 min, before addition to cells. Media was changed 6 h later. Cells were harvested at 24, 48, or 72 h posttransfection for RNA and protein analyses.

Quantitative RT-PCR

From phenol-chloroform extraction, aqueous-phase RNA was precipitated with isopropanol and purified in spin columns of RNeasy kits (Qiagen). RNA (500 ng total) was reverse transcribed using the High-Capacity cDNA

synthesis kit (Thermo Fisher Scientific) and quantified in real time with SYBR Green detector in a QuantStudio 7 Flex (Thermo Fisher Scientific). Relative expressions were calculated by the delta-delta C_T method.

CM-H_2DCFDA Assay

BMSCs were resuspended in Hanks' balanced salt solution, incubated in 10 μmol/L 5-(and-6)-chloromethyl-2′,7′-dichlorodihydrofluorescein diacetate (CM-H_2DCFDA) (Thermo Fisher Scientific) for 45 min at 37°C/5% CO_2/5% O_2, and then analyzed on a BD FACSCalibur.

Fluorogenic ROS Cytochemistry

CellROX (Thermo Fisher Scientific) was added to BMSCs at 5 μmol/L for 30 min at 37°C. Cells were counterstained with DAPI and photographed with an Olympus BX51 microscope.

8-OHdG Measurement

8-Hydroxy-2'-deoxyguanosine (8-OHdG) was measured with Oxidative DNA Damage ELISA Kit (Cell Biolabs, Inc.). Wells of 96-well plates were coated with 100 μL 8-OHdG-BSA/PBS conjugate overnight at 4°C. After washes, plates were blocked with 200 μL assay diluent for 1 h at room temperature. Samples and standards (50 μL) were incubated for 10 min, followed by incubation with 50 μL anti–8-OHdG antibody for 1 h. After washing, 100 μL horseradish peroxidase (HRP)–coupled secondary antibody was incubated for 1 h. After several washes, 100 μL of peroxidase substrate solution was added. The reaction was stopped with 100 μL Stop Solution after 5 min and measured at 450 nm on the Synergy H1 plate reader (BioTek), standardized to total DNA.

Immunocytochemistry

BMSCs were fixed for 10 min using 4% paraformaldehyde/PBS, permeabilized in 0.2% Tween/PBS, and blocked for 30 min in 5% donkey serum (Jackson ImmunoResearch). Nrf2 (ab92946; Abcam) and Keap1 (60027-1-Ig; Proteintech) antibodies were applied and detected with fluorophore-conjugated secondary antibodies. Cells were photographed on an Olympus BX51.

Protein Lysates and Western Blot

Cells were lysed in 10 mmol/L HEPES (pH 7.9), 10 mmol/L KCl, 0.1 mmol/L EDTA, 10 mmol/L dithiothreitol, and 2× protease/phosphatase inhibitor (Sigma-Aldrich). After 15 s vortexing, the lysate was centrifuged at 15,000*g* for 20 min to separate the cytoplasmic extract (supernatant) and nuclear extract (pellet). Cytoplasmic extract was removed into prechilled tubes. The nuclear extract pellet was resuspended in 20 mmol/L HEPES (pH 7.9), 0.4 mol/L NaCl, 1 mmol/L EDTA, 25% glycerol, and 2× protease/phosphatase inhibitor mixture and incubated for 10 min. Nuclear lysate was separated by centrifugation at 15,000*g* for 5 min. Protein concentration was measured using Pierce 660nm Reagent (Thermo Fisher Scientific) on a Nanodrop 2000. Extracts (20 μg) were separated in 12% SDS-polyacrylamide gels and transferred to polyvinylidene fluoride membranes (Bio-Rad). The membrane was blocked for 2 h using 5% nonfat milk/Tris-buffered saline/0.1% Tween (Pierce) and probed with Nrf2, Keap1, PCNA (2586; Cell Signaling Technology), or β-actin (ab8229; Abcam) antibodies. HRP-conjugated secondary antibodies allowed protein detection on hyperfilm (Amersham) with enhanced chemiluminescence plus reagent.

MTT [3-(4,5-Dimethylthiazol-2-yl)-2,5 Diphenyltetrazolium Bromide] Assay

Premixed dye (15 μL) of the CellTiter 96-Cell Proliferation Assay (Promega) was added to cells in 96-well plates for 4 h at 37°C to allow tetrazolium conversion into a formazan product. Solubilization/Stop Solution (100 μL per well) solubilized the formazan product, and the plate was read at 570 nm.

Nrf2 ELISA

Nuclear and cytoplasmic extracts were prepared using the Active Motive Nuclear Extract Kit (no. 40010), and concentrations were measured using Pierce 660nm Reagent on Nanodrop 2000. Activated Nrf2 levels were determined using the TransAm Nrf2 ELISA kit (no. 50296). Plates (96 well) that were coated with an antioxidant response element consensus sequence oligonucleotide were blocked with dithiothreitol/herring sperm DNA buffer. Samples and positive controls (10 μL) were added to wells, followed by Nrf2 antibody for 1 h incubation at room temperature. HRP-conjugated secondary antibody (100 μL) was added per well for 1 h at room temperature. The ELISA was developed by sequentially adding 100 μL each of Developing and Stop Solution per well and reading the plate at 450 nm (reference 655 nm). Nrf2 quantity was based on the positive control.

Keap1 ELISA

Nuclear and cytoplasmic lysates (100 μL) were added to Keap1 antibody–coated plates (ABIN1980574) for 2 h at 37°C. After sample removal, 100 μL Detection Reagent A was added per well for 1 h at 37°C. Detection Reagent B (100 μL) was added to each well for 30 min at 37°C. After washes, 90 μL substrate was added per well and incubated for 15–25 min at 37°C to allow the liquid to turn blue. Stop Solution (50 μL) turned the liquid yellow and the plate was read at 450 nm. Keap1 quantities were calculated based on a standard curve created with recombinant protein in the kit.

GSH/GSSG Assay

GST converts a luminogenic GSH (reduced) probe, luciferin-NT, to luciferin. BMSCs were lysed to release GSH and GSSG (oxidized). The lysis buffer for one set contained *N*-ethylmaleimide to block GSH, allowing luminescence from only GSH reduced from GSSG. Luminescence readings from the total glutathione and only GSSG were used to calculate the GSH/GSSG values.

Cellular Metabolism Assay

Agilent Seahorse Cell Mito Stress Kit was used. In brief, 60,000 cells were seeded in Seahorse XF24 microplates, in low-serum media to prevent changes in cell numbers. One hour before measurement of the oxygen consumption rate and extracellular acidification rate, cells were washed with and switched to Seahorse Assay Medium (5 mmol/L or 25 mmol/L glucose by cell type, 2 mmol/L L-glutamine, no bicarbonate) and incubated without CO_2 to remove any traces. Data were collected at baseline and at intervals after sequential addition of inhibitors oligomycin (1 μmol/L), carbonyl cyanide p-trifluoromethoxy-phenylhydrazone (FCCP) (2 μmol/L), and rotenone/antimycin A (0.5 μmol/L). After data collection, cells were counterstained and fixed. The plate was imaged using the Arrayscan VTI Acquisition Only protocol by collecting nine tiles at 5× magnification and 2 × 2 pixel binning. Images were analyzed using the Morphology Explorer protocol (version 4). Object identification was performed using 3D surface background subtraction, dynamic isodata thresholding of −0.5, and segmented by shape = 2 with object cleanup enabled. Objects touching the border of the image field were rejected from analysis. Between one and four fields per well were used to calculate the average number of cells per field area and used to extrapolate total cell counts in the entire well. Data were normalized to cell number.

Wounding and BMSC Seeding

Full-thickness wounds (10 mm) were created on mice dorsum and then splinted open with 10-mm-diameter silicone stents that were secured by interrupted 4-0 nylon sutures (Ethicon). Photographs of stented wounds were analyzed for percent wound closure (nonhealed wound/original wound), standardized to the internal stent diameter. Area under the curve was calculated using the trapezoidal rule (Graphpad Prism). BMSCs were seeded into wounds with a 20-gauge needle. For histology, 10-day wounds were harvested and fixed, processed into paraffin, sectioned, stained with hematoxylin-eosin or rabbit anti-mouse CD31 antibody (Cell Signaling Technology), and scanned. Blood glucose was measured once a week to ensure diabetic mice retained ≥400 mg/dL glucose throughout the study period.

Statistical Analysis

Data are expressed as mean ± SD of at least three separate trials, each $n = 3$. Student t tests and one-way ANOVA were used. P values <0.05 determined statistical significance.

RESULTS

Diabetic BMSCs Exhibit Altered Identity and Compromised Multipotency

To investigate whether diabetes induces changes in BMSCs, we compared immunophenotypes of BM aspirates between WT and *db/db* mice. Based on lack of expression of the hematopoietic markers CD45 and Ter119, we identified 0.45% and 0.19% BMSCs in WT and *db/db*, respectively (Fig. 1*A*). We analyzed the expression of Sca-1 and PDGFRα, as the combination enriches for BM-resident mesenchymal stem cells (17). $CD45^-Ter119^-Sca\text{-}1^+PDGFR\alpha^+$ BMSCs comprised 0.16% of the WT BM aspirate but only 0.072% of that of *db/db* mice (Fig. 1*B*). The 55% reduction in both $CD45^-Ter119^-$ and $Sca\text{-}1^+PDGFR\alpha^+CD45^-Ter119^-$ cells in *db/db* BM aspirates compared with that of WT indicates a compromised dBMSC pool, including a reduced number of mesenchymal stem cells. Analysis of passage 3 (P3) BM cells showed that the percentage of $CD45^-Ter119^-$ cells was consistently lower in *db/db* cultures (Supplementary Fig. 1*A*). Of $CD45^-Ter119^-$ cells, the percentages of *db/db* $Sca\text{-}1^+$ and $PDGFR\alpha^+$ cells were 28.3% and 64% less than that of WT (Supplementary Fig. 1*B*), respectively, whereas the *db/db* $Sca\text{-}1^+PDGFR\alpha^+$ fraction was only 8.47% of that of WT by P3 (Fig. 1*C*). The expression of other cell surface markers associated with the BM stromal fraction revealed downregulation of CD29 and CD44 in P3 dBMSCs versus P3 WT-BMSCs but upregulation of CD73 (Supplementary Fig. 1*C*).

We then assessed whether the diabetic hyperglycemic conditions affect other multipotency characteristics. Single-cell colony-forming assays revealed 12 ± 4 colony-forming units (CFUs) with dBMSCs, compared with 28.5 ± 2.5 CFUs with WT-BMSCs at P1 (Fig. 1*D*). At P2, we observed 6.5 ± 1.5 dBMSC CFUs and 30.5 ± 1.5 WT-BMSC CFUs. At equivalent passages, dBMSCs had a greater number of flat, polygonal cells (55%) (Fig. 1*F*) and a lower number of spindle-shaped cells, compared with WT-BMSCs (Fig. 1*E*). Flow cytometry forward scatter also revealed that dBMSCs had larger nuclei, compared with WT-BMSC nuclei (Fig. 1*G*). The larger morphology and nuclei are both indicative of differentiated cells. We then cultured both WT and *db/db* BMSCs in adipogenic, osteogenic, or chrondrogenic media. dBMSCs could only successfully differentiate into adipocytes (Fig. 1*H*), indicating that diabetes precludes osteogenic and chondrogenic differentiation capacities. Our results reveal that in diabetic hyperglycemic conditions, phenotypic and behavioral changes in BMSCs reflect their altered identity.

Lack of Nrf2 Activity in Diabetic BMSCs Corresponds With Dysfunction in ROS Management

To determine whether the lack of BMSC characteristics in diabetic mice corresponds with metabolic shifts, we assessed live ROS levels in dBMSCs, WT-BMSCs, and stromal cells. ROS levels in dBMSCs were 3.34-fold higher than in WT-BMSCS (Fig. 2*A* and *B*). Between WT-BMSC and stromal cells, WT-BMSCs contained significantly lower ROS (Fig. 2*C*), suggesting that dBMSCs are more similar to stromal cells than to WT-BMSCs. dBMSCs displayed high levels of nonreduced ROS in the cytoplasm (Fig. 2*D*). Small spindle-shaped dBMSCs showed nuclear and mitochondrial accumulation of ROS (Fig. 2*E*). The larger polygonal dBMSCs only showed cytoplasmic ROS (Fig. 2*D*). ROS generation is associated with oxidative phosphorylation, which is observed in differentiated cells unlike glycolysis in primitive cell populations (7). To determine

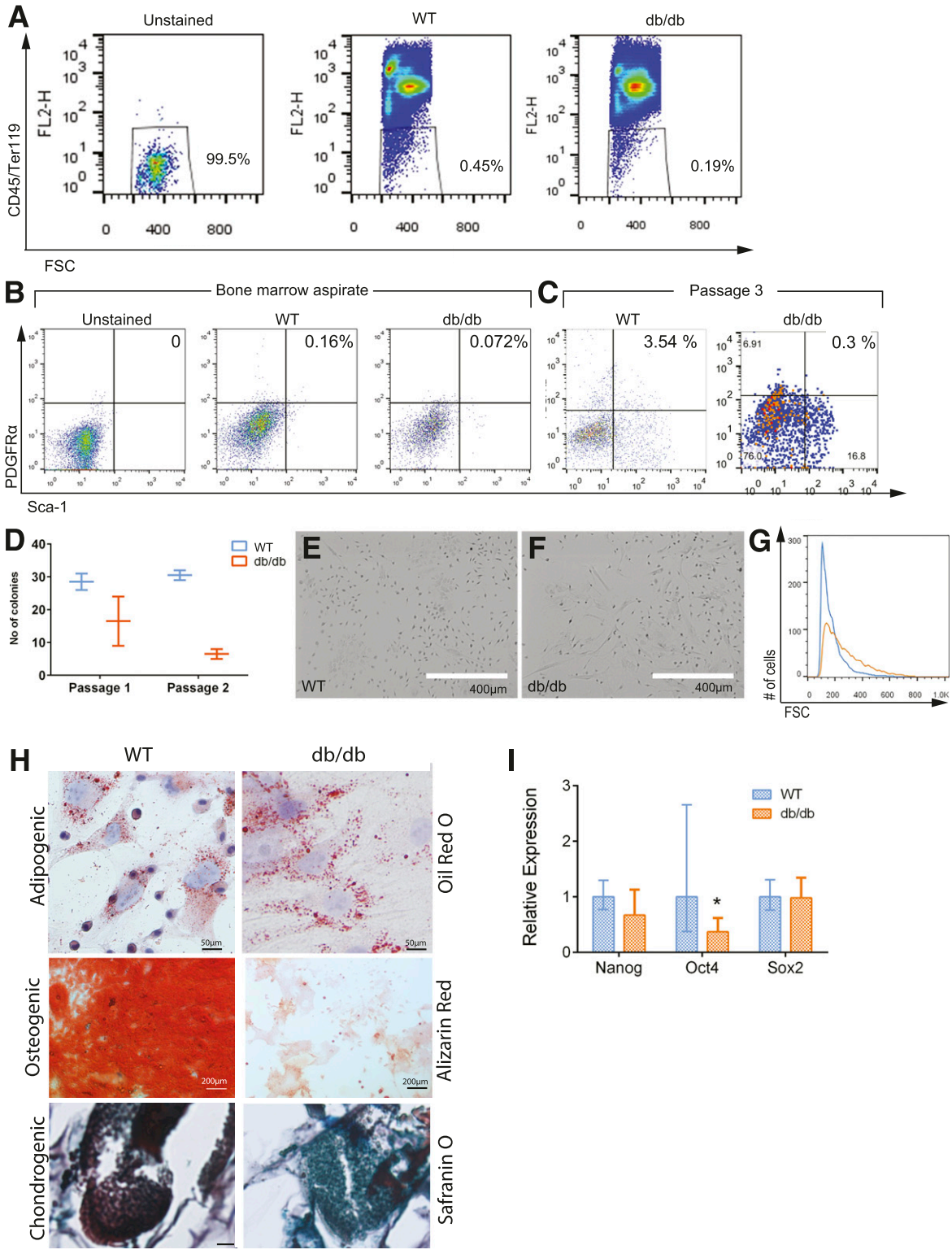

Figure 1—dBMSCs demonstrate reduced multipotent cell characteristics. *A*: Nonhematopoietic fractions of BM aspirates between WT and *db/db* mice. *B*: Phenotypic comparison of CD45$^-$/Ter119$^-$/PDGFRα^+/Sca-1$^+$ BMSCs in WT and *db/db* BM aspirates using cell surface markers. *C*: CD45$^-$/Ter119$^-$/PDGFRα^+/Sca-1$^+$ BMSCs in P3 cell culture. *D*: Single cell–based colony-forming assay. *E* and *F*: Morphology of WT and dBMSCs in culture. *G*: Comparison of nuclei size between WT and dBMSCs. *H*: Stained WT and dBMSCs after 14 days in differentiation media as indicated. Bottom panel scale bar = 100 μm. *I*: Gene expression of pluripotency genes. Data represented as mean ± SD; $n \geq 3$. *$P < 0.05$. See also Supplementary Fig. 1. FSC, forward scatter.

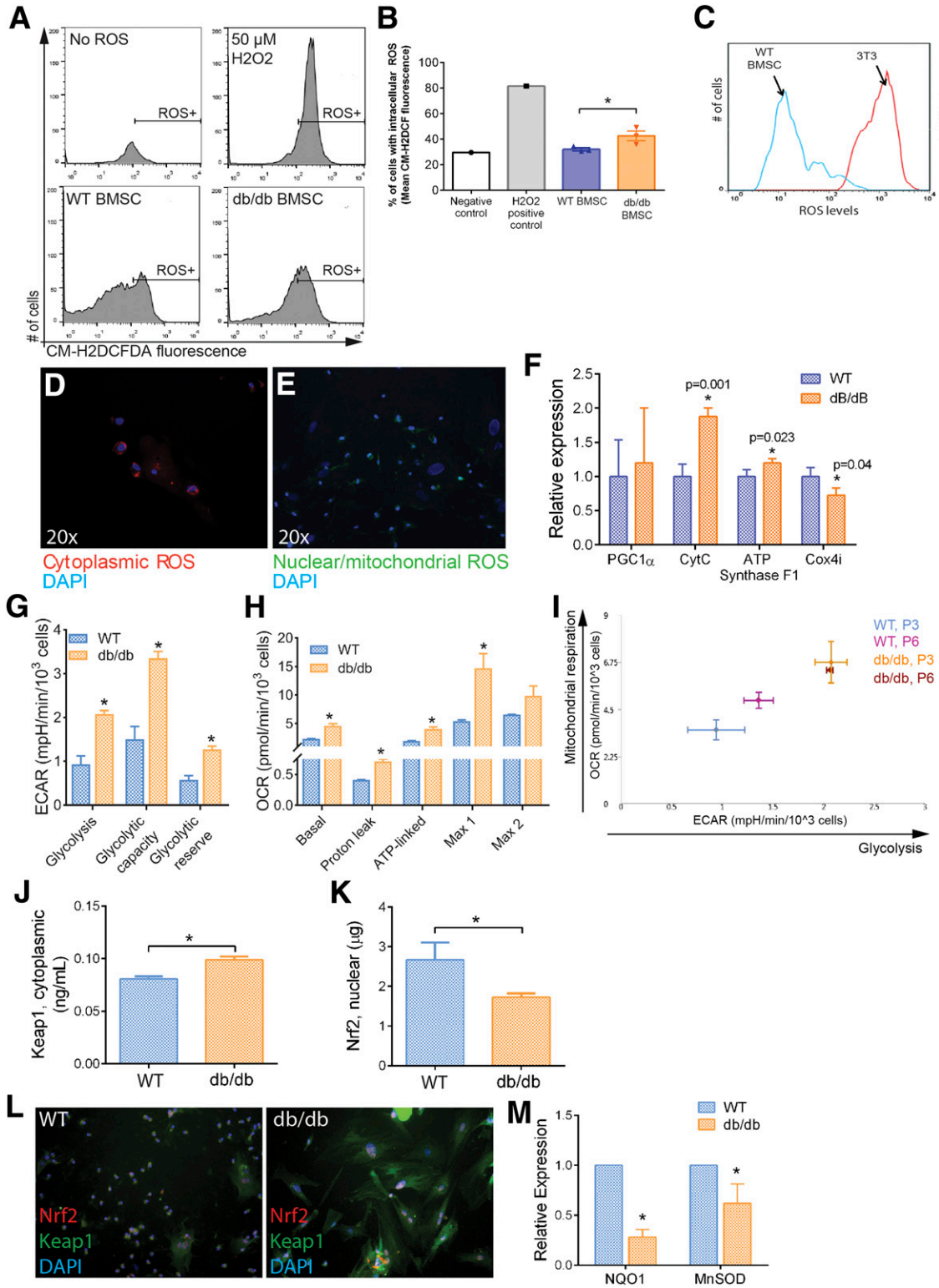

Figure 2—Nrf2/Keap1 pathway affected in altered dBMSCs. *A*: Detection of intracellular ROS using CM-H_2DCFDA. ROS induces deacetylation of cell-permeant CM-H_2DCFDA to fluorescent DCF (Ex/em 492–495/517–527 nm) that is trapped. *B*: Quantification of intracellular ROS. *C*: Comparison of ROS levels between WT-BMSCs and stromal cells using CM-H_2DCFDA. *D* and *E*: Fluorogenic detection of ROS in cytoplasm (red) and nuclei and mitochondria (green). *F*: Gene expression of oxidative phosphorylation genes. *G*: Glycolytic indices, derived from Seahorse Mito Stress analysis. *H*: Mitochondrial respiratory indices, derived from Seahorse Mito Stress analysis. *I*: Energy map of WT and dBMSCs, comparison between P3 and P6. *J* and *K*: ELISA of nuclear Nrf2 and cytoplasmic Keap1 using lysates of WT and dBMSCs. *L*: Immunofluorescence of Nrf2 and Keap1 proteins in WT and dBMSCs. Magnification is 20×. *M*: Relative expression of Nrf2 target genes in WT vs. dBMSCs. Data represented as mean ± SD; $n \geq 3$. *$P < 0.05$. See also Supplementary Fig. 2. ECAR, extracellular acidification rate; OCR, oxygen consumption rate.

whether the high ROS in dBMSCs is associated with precocious oxidative phosphorylation and differentiation, we examined the expression of key genes that identify this metabolic state. Gene expressions of CytC and ATP synthase F1, components of the electron transport chain during aerobic respiration, were upregulated in dBMSCs compared with WT-BMSCs (Fig. 2*F*). Interestingly, Cox4i, a subunit of cytochrome oxidase that transfers electrons to oxygen in the final steps of the electron transport chain and prevents buildup of H_2O_2, was downregulated in dBMSCs, compared with WT-BMSCs (Fig. 2*F*). For a functional readout, we analyzed bioenergetic profiles of WT and dBMSCs and found consistently higher glycolytic indices in similar numbers of dBMSCs than WT-BMSCs (Fig. 2*G* and Supplementary Fig. 2*A*). Mitochondrial respiration rates demonstrated that dBMSCs had significantly higher oxidative phosphorylation indices than WT-BMSCs (Fig. 2*H* and Supplementary Fig. 2*B*). However, dBMSCs also demonstrated sharp depletion of mitochondrial reserve capacity with a second addition of carbonyl cyanide p-trifluoromethoxyphenylhydrazone, which maximizes respiration steadily in WT-BMSCs (Max 2) (Fig. 2*H*). Combining glycolytic and mitochondrial respiration profiles indicates that dBMSCs do not display the glycolytic profile seen in WT-BMSCs and characteristic of progenitor cells. Of interest, increasing passages of WT-BMSCs demonstrated a shift away from a glycolytic profile as well, toward that of dBMSCs (Fig. 2*I*).

As the Nrf2/Keap1 pathway would typically manage ROS burdens, we analyzed key components. Protein expression demonstrated that Nrf2 is less abundant in nuclei of dBMSCs, compared with WT-BMSCs (Fig. 2*J*). Concurrently, Keap1 is strongly upregulated in dBMSC cytoplasm, compared with WT-BMSCs (Fig. 2*K*). Immunocytochemistry showed significant upregulation in cytoplasmic Keap1 in dBMSCs compared with that of WT-BMSCs (Fig. 2*L*). *NQO1* and *MnSOD* gene expression showed significant downregulation in dBMSCs (Fig. 2*M*). Due to disruption of the Nrf2/Keap1 antioxidant pathway in diabetes, dBMSCs show reduced ability to manage ROS, concomitant with a conspicuous shift away from typical glycolytic metabolism of multipotent cells and toward energetic oxidative phosphorylation seen in differentiated cells. Our results thus far indicate that the uncoupling of ROS accumulation and Nrf2 release from Keap1, and consequently, downregulation of intrinsic Nrf2-mediated redox regulatory mechanisms in dBMSCs, propels differentiation at the cost of multipotency.

Silencing *Keap1* Upregulates Antioxidant Mechanisms in dBMSCs

Based on anomalous levels of Nrf2 and Keap1 in dBMSCs, we analyzed *Keap1* gene expression and found a 1.65 ± 0.1-fold increase in dBMSCs compared with WT-BMSCs (Fig. 3*A*). To restore nuclear Nrf2 activity, we silenced *Keap1* in dBMSCs using siRNA, while cells were still cultured in hyperglycemic conditions. We detected 65 ± 7.9% *Keap1* knockdown compared with untreated dBMSCs and 41.5 ± 1.3% knockdown compared with WT-BMSCs (Fig. 3*A*). With si*Keap1* in WT-BMSCs, cytoplasmic Keap1 protein sharply decreased in contrast to untreated cells (Fig. 3*B* and *C*). In dBMSCs, *Keap1* silencing resulted in remarkable reduction in Keap1 protein as well (Fig. 3*B* and *C*). *Keap1* knockdown in WT-BMSCs and dBMSCs resulted in a significant upregulation of nuclear Nrf2, compared with untreated cells (Fig. 3*B* and *D*). Immunocytochemistry revealed that Nrf2 is present in the nucleus in si*Keap1*-dBMSCs, along with a conspicuous lack of Keap1 in the cytoplasm (Fig. 3*E*). Next, we investigated whether Nrf2 upregulation affects redox homeostasis of dBMSCs. ROS levels of si*Keap1*-dBMSCs diminished significantly, compared with untreated dBMSCs (Fig. 3*F*). *Keap1* inhibition in dBMSCs increased $CD45^-/Ter119^-/Sca\text{-}1^+/PDGFR\alpha^+$ cells to 1.4% (Fig. 3*G*), a nearly fivefold increase from their original numbers (Fig. 1*C*). We then quantified 8-OHdG, a biomarker of oxidative stress, between WT and si*Keap1*-dBMSCs. In dBMSCs, silencing *Keap1* resulted in a significant decrease in 8-OHdG concentrations to near WT levels (Fig. 3*H*). Fluorogenic indicators also confirmed the diminished levels of cytoplasmic ROS in si*Keap1*-dBMSCs, with 32.22 ± 11.24% of si*Keap1*-dBMSCs containing ROS in stark contrast to 86.11 ± 15.26% of dBMSCs (Supplementary Fig. 3).

To assess Nrf2 activity, we examined the expression of key transcripts after *Keap1* silencing. In comparison with untreated dBMSCS, gene expressions of *NQO1* and *MnSOD* were significantly upregulated (Fig. 3*I* and *J*). *Nox4*, known for its protective functions in redox management (18), was upregulated (Fig. 3*K*). Gene expression of other Nrf2-transcribed antioxidant molecules, *HO-1*, glutathione-*S*-reductase (*GSR*), glutathione-peroxidase-1 (*Gpx1*), *GSTμ1*, and *GSTα3*, followed the significant upregulation trend (Supplementary Fig. 4). To further evaluate the metabolic effects of upregulating Nrf2 levels, we assessed the GSH-to-GSSG ratio, an indicator of cellular redox status that is regulated by Nrf2 targets (19). Silencing *Keap1* raised the GSH-to-GSSG ratio in dBMSCs compared with untreated cells ($P < 0.005$), and similar to GSH/GSSG in WT-BMSCs (Fig. 3*L*). These data suggest that restoring expression of the major regulator Nrf2 can resolve the diabetes-induced aberrant intracellular redox homeostasis and metabolic routes in dBMSCs.

Nrf2 Activity Rescues Multipotent Cell Traits in dBMSCs

Having successfully rescued the diabetes-induced disruptions in the Nrf2/Keap1 pathway in dBMSCs, we now assessed the role of Nrf2/Keap1 in cell identity in high ROS. As Nrf2 upregulation increased the percentage of immature dBMSCs, we analyzed their differentiation potential. The quantity of lipids present in native dBMSCs resembled that of purposefully adipogenic-differentiated si*Keap1*-treated ones (Fig. 4*A*, i). This indicates that dBMSCs exhibit precocious adipogenic differentiation. Unlike the absence of red calcium deposits in native dBMSCs, the *Keap1*-silenced cells in osteogenic media

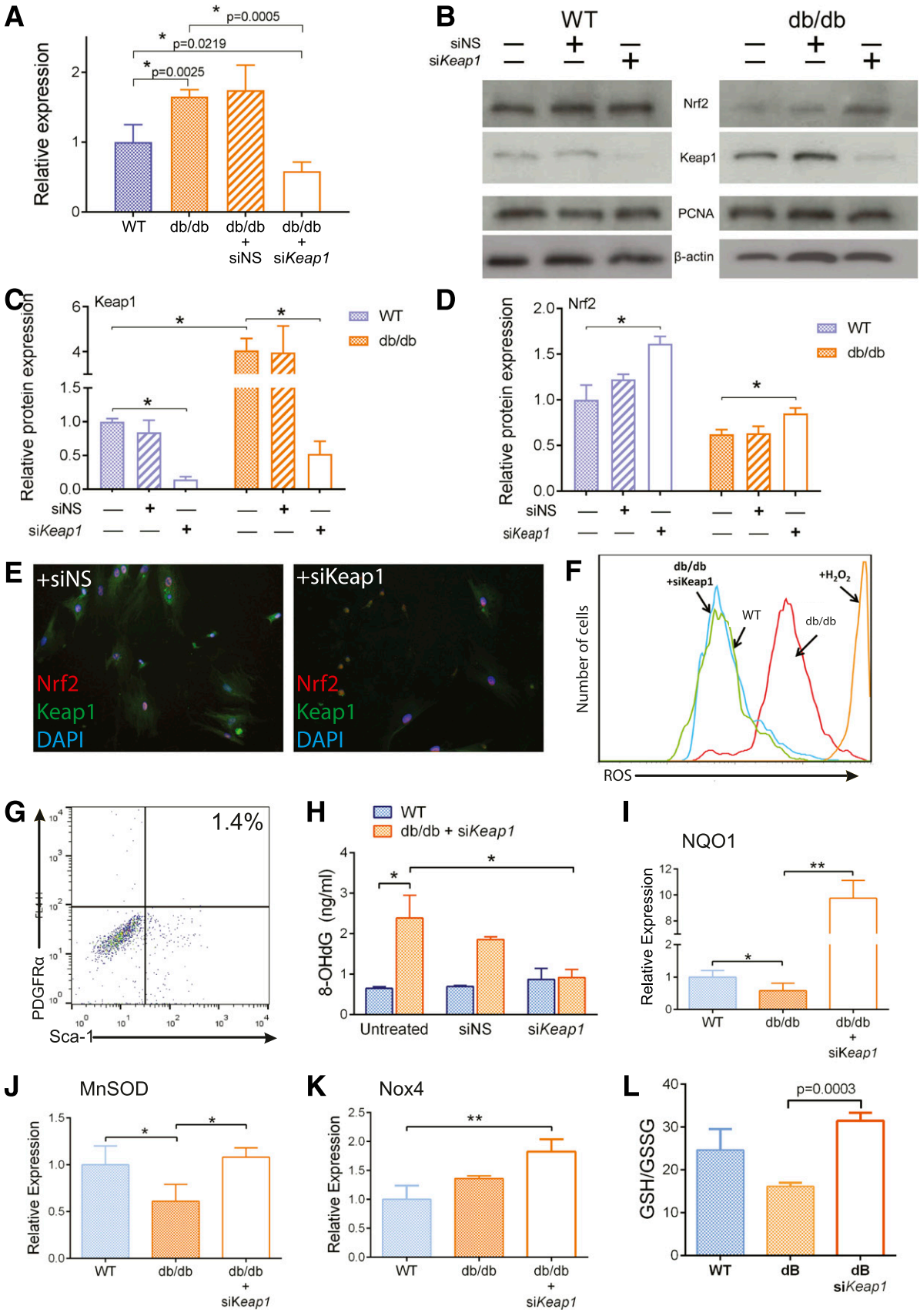

Figure 3—Knockdown of *Keap1* restores Nrf2-mediated antioxidant and metabolic mechanisms in dBMSCs. *A*: Relative expression of *Keap1* after silencing, 24 h posttransfection. NS served as a negative control for transfection. *B*: Immunoblot of nuclear and cytoplasmic lysates of untreated and silenced WT and dBMSCs, 48 h posttransfection. *C* and *D*: Relative protein expression of Nrf2 and Keap1 in cells as

had remarkable staining (Fig. 4*A*, ii). In contrast to native dBMSCS, si*Keap1*-treated cells showed the onset of chondrogenic differentiation (Fig. 4*A*, iii). We further analyzed the expression of genes associated with each lineage among WT-BMSCs, dBMSCs, and si*Keap1*-dBMSCs. At basal stages, the adipogenesis-associated gene adipocyte protein 2 (*aP2*) was similar between WT and dBMSCs (Fig. 4*B*), whereas peroxisome proliferator–activated receptor γ (*PPARγ*) was upregulated in dBMSCs relative to WT-BMSCs (Fig. 4*C*). At 3 days into adipogenic induction, both *aP2* and *PPARγ* were significantly overexpressed in dBMSCs, compared with WT-BMSCs (Fig. 4*B* and *C*). si*Keap1*-dBMSCs significantly reduced both genes. Then, we analyzed osteogenic genes *BMP2*, osterix (*Osx*), and runt-related transcription factor 2 (*RUNX2*). At day 0, *BMP2* expression in dBMSCs was remarkably downregulated, compared with WT-BMSCs (Fig. 4*D*). At day 3 of osteogenic induction, whereas WT-BMSCs showed downregulation of *BMP2*, dBMSCs showed abnormal upregulation. si*Keap1*-dBMSCs reduced *BMP2* expression, similar to WT-BMSCs. Compared with WT-BMSCs, the irregular temporal pattern of gene expression in dBMSCs was apparent with *Osx* and *RUNX2* as well but was restored with si*Keap1* (Fig. 4*E* and *F*). For chondrogenic induction, dBMSCs showed downregulation of collagen type 2αI (*Col2aI*) and aggrecan (*ACAN*) with respect to WT-BMSCs, but with si*Keap1*, gene expression followed the WT-BMSC pattern (Fig. 4*G* and *H*). Our data indicate that activation of Nrf2 is necessary for multilineage differentiation, and this capacity can be restored in dBMSCs.

To evaluate the extent of restoration of typical multipotent cell features in *Keap*1-silenced dBMSCs, we analyzed BMSC migration capacity toward SDF1, as BMSCs express the CXC chemokine receptor 4 (CXCR4) (20). dBMSCs exhibited reduced migratory capacity, compared with WT-BMSCs (Fig. 4*I*). *Keap1* silencing not only rescued this behavior but boosted migration capacity over that of WT-BMSCs (Fig. 4*I*). We explored gene expression of *CycD1* and *CycD2*, which allow cell cycle progression, and found significantly downregulated expression in dBMSCs, compared with WT-BMSCs. *Keap1* inhibition in dBMSCs resulted in statistically significant upregulation of both *CycD1* and *CycD2*, compared with untreated dBMSCs (Fig. 4*J*). Next, we measured the proliferation of WT-BMSCs, dBMSCs, and si*Keap1*-dBMSCs. At all time points after transfection with si*Keap1*, si*Keap1*-dBMSCs had nearly twice the quantity of cells, compared with untreated ones (Fig. 4*K*). Nrf2 activity restored not only multipotency of dBMSCs but their behavioral aspects as well. Our results indicate that BMSCs require functional Nrf2/Keap1 signaling to maintain cell identity in unusual redox conditions, as in diabetes.

Nrf2 Activity in BMSCs Is Coupled to Sox2 Expression

Searching for candidates that further examine the Nrf2-initiated mechanisms in retaining BMSC multipotency, we came across Sox2, which regulates self-renewal and stemness of osteo-adipo lineage cells (21). We analyzed whether *Sox2* expression is affected by modulation in Nrf2 activity. WT-BMSCs and dBMSCs did not show differential expression (Fig. 5*A*). However, a time course analysis after *Keap1* inhibition showed that dBMSCs significantly upregulated *Sox2* expression, particularly at 48 and 72 h, in relation to native dBMSCs (Fig. 5*B*). Additionally, analysis of gene expression of Yes-associated protein 1 (*YAP1*), a direct downstream target and effector of Sox2 (21), showed similar upregulation at 48 and 72 h post-si*Keap1* transfection. To analyze the functional consequence of the transient upregulation of *Sox2* induced by Nrf2, we analyzed the differentiation potential of si*Keap1*-dBMSCs with and without Sox2. We knocked down *Nrf2* using siRNA and/or *Sox2* using short hairpin RNA in WT-BMSCs. We also knocked down *Keap1* and *Sox2* in dBMSCs, in si*Keap1*-dBMSCs. After 2 weeks in osteogenic media, si*Nrf2*-WT-BMSCs showed poor alizarin red staining, indicating poor osteogenesis (Fig. 5*C*). WT-BMSCs with both *Nrf2* and *Sox2* knockdown displayed similar failure. In dBMSCs, the simultaneous knockdown of *Sox2* and *Keap1* negated the osteogenic capacity induced by only *Keap1* inhibition. Our results suggest that Sox2 and YAP are necessary to impart the BMSC multipotency that is regulated by Nrf2 and compromised in diabetes.

Lack of Nrf2/Keap1 Signaling in dBMSCs Limits Their Role in Tissue Regeneration

As BMSCs orchestrate repair/regeneration in a wound setting (3), we assayed the impact of Nrf2/Keap1 activity on this capacity using cultured BMSCs in a previously established wound model (22). We seeded the wound with BMSCs and monitored time to closure as a readout of BMSC function during repair (Fig. 6*A*). The addition of any BMSCs provided an advantage to diabetic wound closure and healing. The addition of short interfering nonsense (siNS)-dBMSCs accelerated healing time to 25.5 ± 2.12 days, compared with untreated diabetic wounds at 31.25 ± 1.5 days (Fig. 6*B*–*D*). Wounds with WT-BMSCs and si*Keap1*-dBMSCs demonstrated that the most significant reduction in wound healing time was 22 ± 2.4 days and 20.75 ± 2.36 days, respectively (Fig. 6*B* and *C*). These data indicate that Nrf2 induction by si*Keap1* enables dBMSCs to successfully coordinate tissue

indicated. *E*: Immunofluorescence of Nrf2 and Keap1 in dBMSCs transfected with siNS or si*Keap1*. Magnification is 20×. *F*: Flow cytometric analysis of intracellular ROS of indicated cells after *Keap1* silencing, using CM-H_2DCFDA. *G*: Percentage of PDGFRα$^+$/Sca-1$^+$ dBMSCs after si*Keap1* application. *H*: Quantification of 8-OHdG adducts, an indicator of ROS-mediated DNA damage. *I*–*K*: Quantitative RT-PCR of Nrf2-transcribed genes as indicated. *L*: Total glutathione in cells. Data represented as mean ± SD; $n \geq 3$. *$P < 0.05$; **$P < 0.01$. See also Supplementary Figs. 3 and 4.

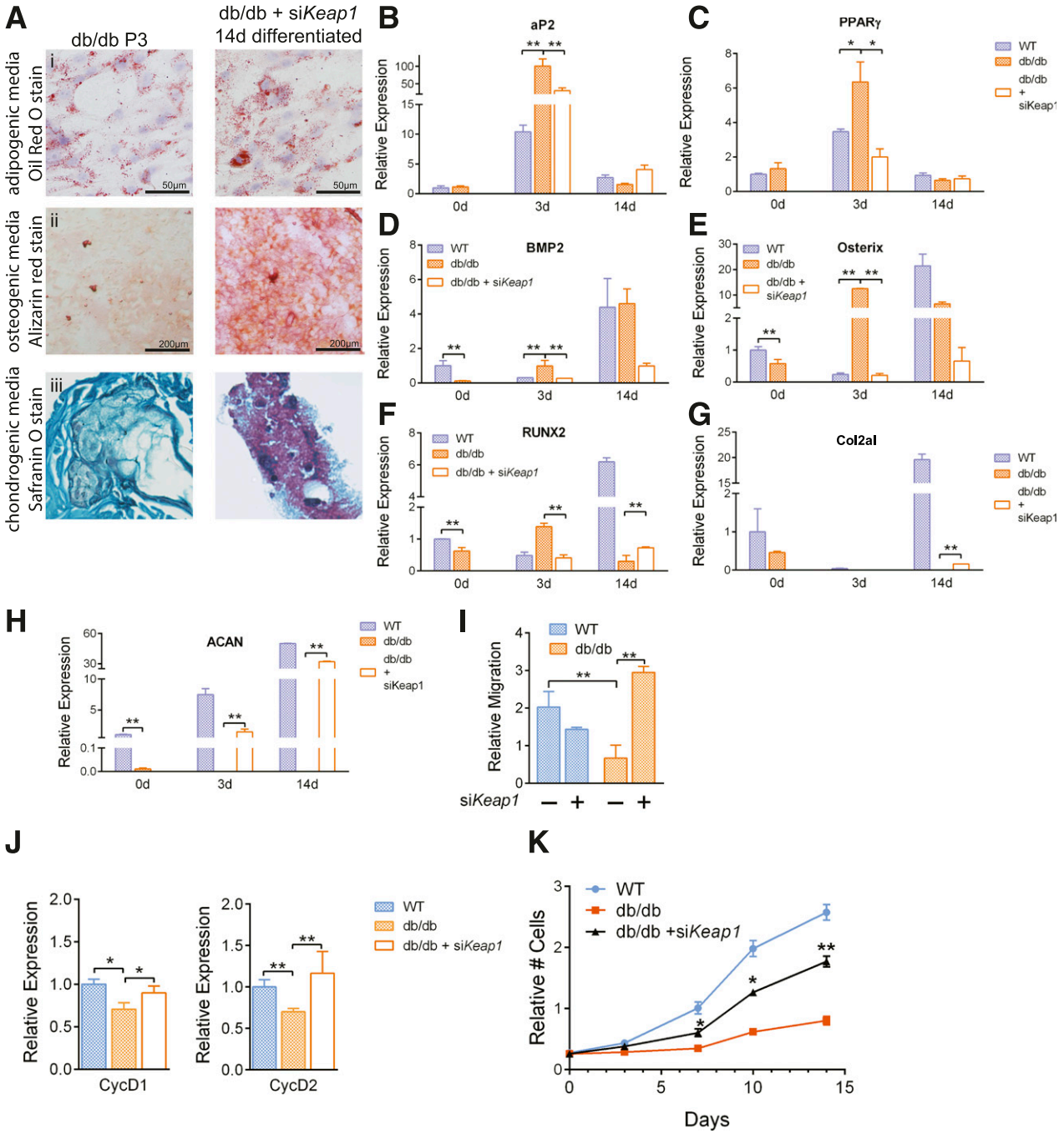

Figure 4—Nrf2 activation restores multipotency in dBMSCs. *A*: Stained *db/db* and si*Keap1*-dBMSCs at P3 and 14 days in differentiation media as indicated. Panel iii magnification is 20×. *B* and *C*: Relative expression of adipogenic genes. *D–F*: Relative expression of osteogenic genes. *G* and *H*: Relative expression of chondrogenic genes. *I*: Transwell migration assay using WT or dBMSCs as indicated. *J*: Relative expression of cell cycle regulators. *K*: Proliferation in cells using MTT assay. Data represented as mean ± SD; $n \geq 3$. *$P < 0.05$; **$P < 0.01$.

repair, like WT-BMSCs. For diabetic wounds with si*Keap1*-BMSCs, the decrease in pathological wound burden correlated with the significant decrease in time to closure (Fig. 6*C* and *D* and Supplementary Fig. 5*A*). Wound healing rates further highlight the impact of seeding si*Keap1*-dBMSCs to diabetic wounds in comparison with untreated wounds (Supplementary Fig. 5*B*). As BMSCs exert their repair role in the granulation tissue, we analyzed tissue sections of the wound bed. WT and si*Keap1*-dBMSCs promoted larger areas of granulation tissue in the healing edges compared with siNS-dBMSC–treated diabetic wounds (Fig. 6*E*). In addition, WT and si*Keap1*-dBMSCs significantly increased $CD31^+$ neovascularization in the granulation tissue, compared with siNS cells (Fig. 6*F*), a feature that BMSCs typically contribute to during repair (23). Isotype controls for the primary antibodies failed to show any

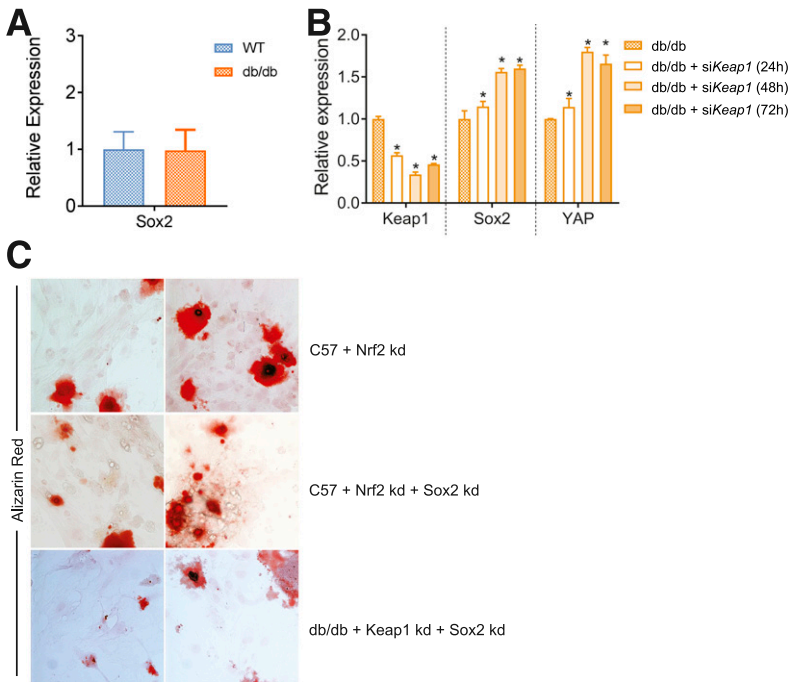

Figure 5—BMSC multipotency dependent on restoration of Sox2 expression. *A*: Relative expression of Sox2. *B*: Time course of relative expression of Sox2 and YAP after *Keap1* knockdown. *$P < 0.05$, in comparison with untreated dBMSCs. *C*: Alizarin red staining of BMSCs as indicated, after 2 weeks in osteogenic media. Magnification is 20×. kd, knockdown.

immunoreactivity (data not shown). Our data demonstrate that restoration of the Nrf2/Keap1 signaling axis in dBMSCs normalizes their capacity to facilitate tissue regeneration, even in an environment presenting extracellular redox stresses.

DISCUSSION

Knowledge of molecular regulators and their deficits in diabetes is critical to enable specificity and efficacy in therapeutic approaches. We previously showed that lack of tissue repair in the extreme redox imbalance of diabetic wound healing is due to dysregulated Nrf2/Keap1 signaling (5). As BMSCs contribute to wounds with oxidative stress to limit tissue damage and promote tissue regrowth (3,24), we explored the effect of diabetes on BMSCs. We established that Nrf2-mediated transcription in BMSCs influences cellular metabolism through redox management to affect differentiation status.

We found diabetes induced unusually high ROS accumulation in dBMSCs, similar to reported diabetic bone marrow–derived cells (25), along with significantly increased Keap1 expression and downregulation of Nrf2 and downstream redox enzymes. Normalization of Nrf2/Keap1 levels produced upregulation of antioxidant enzymes, diminishing ROS levels, and restoration of metabolism in dBMSCs. 8-OHdG decreased and GSH/GSSG increased to WT levels, possibly due to Nrf2-regulated DNA repair enzymes (26) and transcription of GCL catalytic subunits, respectively (13). Low GSH in dBMSCs is likely exacerbated by the polyol pathway in diabetes, due to lack of NADPH also regulated by Nrf2/Keap1 (2,27). We show that Nrf2/Keap1 is a major determinant of low ROS, a known requirement in glial progenitors and HSCs (28,29). This redox management is conserved across vertebrate and invertebrate HSCs (30,31) and intestinal stem cells (ISCs) (32). Activation of the Nrf2/Keap1 pathway mitigates oxidative stress in adult mouse BMSCs in their native state and prevents multifaceted metabolic deficiencies but is severely compromised with the extrinsic environment in diabetes.

Lack of multipotency in dBMSCs corresponded to phenotypic and morphological features of differentiated cells and expression of oxidative phosphorylation genes. A preference for glycolysis in WT-BMSCs is not surprising given the hypoxic nature of BM. However, dBMSCs exhibited metabolic profiles associated with differentiated cells as well, such as high energy-producing oxidative phosphorylation. The high ATP-linked respiration and higher basal respiration in dBMSCs, together with proton leak and less Cox4i, with higher ROS may explain this observation. Premature differentiation in diabetes possibly limits the pool of self-renewing BMSCs. Forced downregulation of Keap1 and thus Nrf2 activation, and subsequent Sox2 expression, reverted the adipogenic differentiation bias in dBMSCs and enabled them to respond to distinct lineage induction cues in culture. Sox2 is a sensitive transcription factor, well recognized for its role in maintenance of multipotency in osteoblasts (21) and proliferation potential (33). Similar to our findings of the deficiencies in dBMSCs, Nrf2 and Sox2 are required for proliferation in glioma stem cells (34). A well-tuned homeostatic balance of Keap1 and Nrf2 is obviously vital,

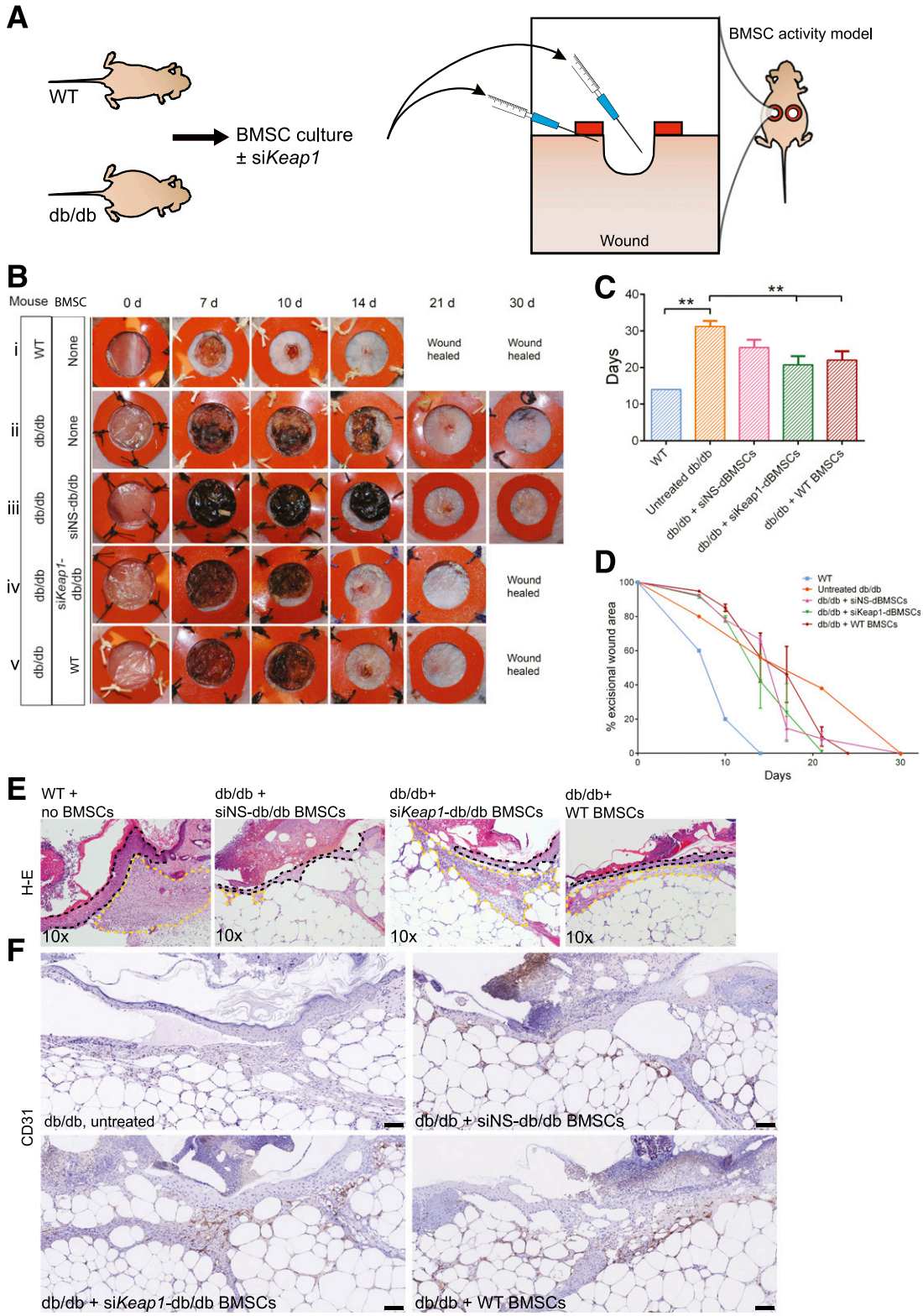

Figure 6—si*Keap1*-transfected dBMSCs reconstitute role in repair. *A*: BMSCs from WT or *db/db* mice were cultured and prepared 24 h prior, with or without transfection with si*Keap1*. Twenty-four hours postexcision, 5,000,000 cells in 300 μL were injected into the cutaneous wound bed and immediate periphery. The wound bed was seeded with 100 μL, and the remaining 200 μL was seeded in 50-μL aliquots in the immediate wound periphery. *B*: Photographs of excisional wounds inoculated with BMSCs as indicated. *C*: Mean time to closure of cutaneous wounds. *D*: Photometric quantification of wound area. *E*: Hematoxylin-eosin stains of tissue sections of 10-day wounds. Wound is to the left in the image. Dashed black line, wound edge epidermis. Yellow lines delineate granulation tissue area. *F*: CD31 immunohistochemistry on 10-day wound tissue. Scale bars, 100 μm. Data represented as mean ± SD; $n = 4$. $^{**}P < 0.01$. See also Supplementary Fig. 5.

as loss of Keap1 has been shown to lead to hyperproliferation. Nrf2 is known to regulate SIRT1, which posttranslationally regulates Sox2 in human bone marrow–derived mesenchymal stem cells (35). Metabolic changes in pluripotent and cancer cells have been shown to alter their cell differentiation status (36), not unlike the changes in diabetes. Mitochondrial ROS accumulation is sufficient to trigger adipocyte differentiation in human BMSCs (37) to resemble dBMSCs. ROS in fact primes *Drosophila* HSCs for a specific lineage (30). Similar to our approach, the authors prevent *Drosophila* HSC differentiation by neutralizing ROS. Even in a whole organ, such as the mouse liver, Nrf2 negatively regulates lipid biosynthetic mechanisms (38). Our results would then indicate that Nrf2/Keap1 signaling is required to preserve the multipotency of BMSCs in cooperation with Sox2. In diabetes, long-term hyperglycemia and persistent downregulation of Nrf2 signaling via Keap1 is a switch for adipogenic differentiation.

Improvement in time to closure of diabetic wounds when seeded with Nrf2-activated dBMSCs illustrated the link between redox and multipotency status of BMSCs and their ability to coordinate successful healing. Muted Nrf2/Keap1 signaling in dBMSCs negatively affected migratory capacity and proliferation in culture, to possibly affect mobilization of BMSCs into injury sites and insufficient healing events in diabetic tissues. A supporting study found that neovascularization was impaired in diabetes models due to defective adipose-derived MSCs (24). We demonstrate that metabolic shifts that characterize diseases like diabetes trickle down to the level of stem/progenitor cells, crippling their populations, identity, and behavior to limit regenerative ability. Existing literature describes the detrimental effects of diabetes and hyperglycemia, such as depletion of endothelial precursor cells, as irreversible through glycemic control (39). Focusing on the mechanisms that modulate metabolism offers options

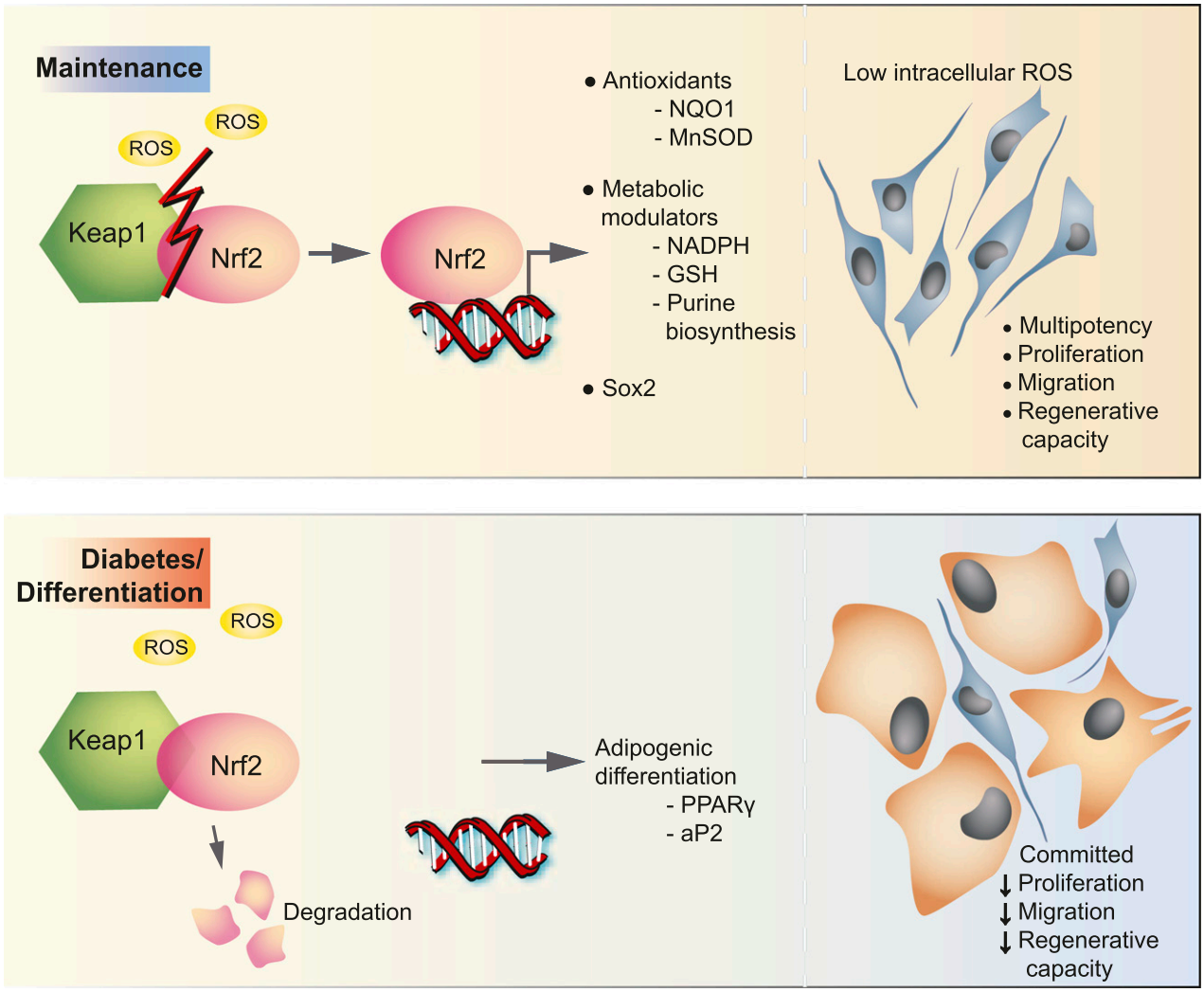

Figure 7—Model for regulation of BMSCs by the Nrf2/Keap1 pathway and disruption in diabetes. In steady state, activation of the Nrf2/Keap1 pathway preserves redox metabolism, multipotency, and associated features of BMSCs. Nrf2 drives transcription of antioxidants, metabolic modulators, and Sox2 to maintain low ROS in BMSCs and maintain multipotency. In diabetes, loss of Nrf2-driven transcription, and therefore high intracellular ROS, promotes expression of adipogenic genes and leads to commitment of BMSCs to an adipogenic fate.

to rescue these detrimental changes at a cellular level at least. The hyperglycemia-induced ROS accumulation can be restored at a local tissue (5) and cellular level.

Our study strongly indicates that coinduction of the redox and metabolism modulatory roles of the Nrf2/Keap1 pathway governs the identity of mouse BMSCs. We showed that diabetes diminishes properties and alters cell fates of BMSCs by unhinging the endogenous Nrf2/Keap1-mediated antioxidant mechanisms that are at the core of ROS management (Fig. 7). The lack of Nrf2 signaling reprograms metabolism in dBMSCs to add to ROS mismanagement and indicates a need for low ROS for maintenance. In *Drosophila*, constitutive Nrf2 or CncC activation limits proliferation of ISCs by keeping ROS in check (32). In response to injury and regenerative need, Keap1 represses CncC to induce proliferation. Though mouse BMSCs require Nrf2 activation to proliferate in very obvious discrepancy with *Drosophila* ISCs, Nrf2 activation maintains the stem cell pool in ISCs and our BMSC model. In-depth understanding of the metabolic changes in BMSC regulation will allow us to address diabetic complications and design rescues for desired outcomes. In a departure from traditional signaling and growth factors in cell lineage, we show evidence that the Nrf2/Keap1 pathway has a much broader cytoprotective role in BMSCs than appreciated, encompassing redox homeostasis and metabolic modulation to determine cell identity and maintenance.

Acknowledgments. The authors are very grateful to Camille Kim, Rita Abigail Sartor, and Bukhtawar Waqas (all from New York University) for assistance with BM harvests. The authors thank Dr. Alka Mansukhani and Dr. Narendra Verma (both from New York University) for sharing the shSox2 vector components. The authors thank Dr. Morris Birnbaum (Pfizer) for critical reading of the manuscript.

Funding. This study was partially supported by an New York University Kimmel Stem Cell training grant to M.A.S. and American Diabetes Association Pathway Award 1-16-ACE-08 to D.J.C. The authors are grateful to the Cytometry and Cell Sorting Core, Experimental Pathology Core, Microscopy Core, and High Throughput Biology Core at NYU Langone Medical Center, supported in part by the Laura and Isaac Perlmutter Cancer Center Support grant National Institutes of Health (NIH)/National Cancer Institute P30CA016087, the NIH grants S10 OD010584-01A1 and S10 OD018338-01, NYSTEM contract C026719, and the Helen L. and Martin S. Kimmel Center for Stem Cell Biology.

Duality of Interest. No potential conflicts of interest relevant to this article were reported.

Author Contributions. P.S.R. designed and performed experiments, analyzed data, and wrote and reviewed the manuscript. M.A.S. designed and performed experiments and analyzed data. S.G.H., R.L.K., A.M., and M.K. assisted with experiments. D.J.C. reviewed the manuscript. P.S.R. and D.J.C. are the guarantors of this work and, as such, had full access to all the data in the study and take responsibility for the integrity of the data and the accuracy of the data analysis.

References

1. Houstis N, Rosen ED, Lander ES. Reactive oxygen species have a causal role in multiple forms of insulin resistance. Nature 2006;440:944–948

2. Giacco F, Brownlee M. Oxidative stress and diabetic complications. Circ Res 2010;107:1058–1070

3. Malhotra S, Hu MS, Marshall CD, et al. Mesenchymal stromal cells as cell-based therapeutics for wound healing. *Stem Cells Int* 2016;2016:4157934

4. Ceradini DJ, Yao D, Grogan RH, et al. Decreasing intracellular superoxide corrects defective ischemia-induced new vessel formation in diabetic mice. J Biol Chem 2008;283:10930–10938

5. Soares MA, Cohen OD, Low YC, et al. Restoration of Nrf2 signaling normalizes the regenerative niche. Diabetes 2016;65:633–646

6. Wanet A, Arnould T, Najimi M, Renard P. Connecting mitochondria, metabolism, and stem cell fate. Stem Cells Dev 2015;24:1957–1971

7. Ito K, Suda T. Metabolic requirements for the maintenance of self-renewing stem cells. Nat Rev Mol Cell Biol 2014;15:243–256

8. Cipolleschi MG, Dello Sbarba P, Olivotto M. The role of hypoxia in the maintenance of hematopoietic stem cells. Blood 1993;82:2031–2037

9. Hermitte F, Brunet de la Grange P, Belloc F, Praloran V, Ivanovic Z. Very low O2 concentration (0.1%) favors G0 return of dividing CD34+ cells. Stem Cells 2006;24:65–73

10. Fehrer C, Brunauer R, Laschober G, et al. Reduced oxygen tension attenuates differentiation capacity of human mesenchymal stem cells and prolongs their lifespan. Aging Cell 2007;6:745–757

11. Rochefort GY, Delorme B, Lopez A, et al. Multipotential mesenchymal stem cells are mobilized into peripheral blood by hypoxia. Stem Cells 2006;24:2202–2208

12. Kensler TW, Wakabayashi N, Biswal S. Cell survival responses to environmental stresses via the Keap1-Nrf2-ARE pathway. Annu Rev Pharmacol Toxicol 2007;47:89–116

13. Hayes JD, Dinkova-Kostova AT. The Nrf2 regulatory network provides an interface between redox and intermediary metabolism. Trends Biochem Sci 2014;39:199–218

14. Chen CT, Shih YR, Kuo TK, Lee OK, Wei YH. Coordinated changes of mitochondrial biogenesis and antioxidant enzymes during osteogenic differentiation of human mesenchymal stem cells. Stem Cells 2008;26:960–968

15. Mohammadzadeh M, Halabian R, Gharehbaghian A, et al. Nrf-2 overexpression in mesenchymal stem cells reduces oxidative stress-induced apoptosis and cytotoxicity. Cell Stress Chaperones 2012;17:553–565

16. Evans JL, Goldfine ID, Maddux BA, Grodsky GM. Are oxidative stress-activated signaling pathways mediators of insulin resistance and beta-cell dysfunction? Diabetes 2003;52:1–8

17. Houlihan DD, Mabuchi Y, Morikawa S, et al. Isolation of mouse mesenchymal stem cells on the basis of expression of Sca-1 and PDGFR-α. Nat Protoc 2012;7:2103–2111

18. Kovac S, Angelova PR, Holmström KM, Zhang Y, Dinkova-Kostova AT, Abramov AY. Nrf2 regulates ROS production by mitochondria and NADPH oxidase. Biochim Biophys Acta 2015;1850:794–801

19. Mitsuishi Y, Taguchi K, Kawatani Y, et al. Nrf2 redirects glucose and glutamine into anabolic pathways in metabolic reprogramming. Cancer Cell 2012;22:66–79

20. Son BR, Marquez-Curtis LA, Kucia M, et al. Migration of bone marrow and cord blood mesenchymal stem cells in vitro is regulated by stromal-derived factor-1-CXCR4 and hepatocyte growth factor-c-met axes and involves matrix metalloproteinases. Stem Cells 2006;24:1254–1264

21. Seo E, Basu-Roy U, Gunaratne PH, et al. SOX2 regulates YAP1 to maintain stemness and determine cell fate in the osteo-adipo lineage. Cell Reports 2013;3:2075–2087

22. Galiano RD, Michaels Jt, Dobryansky M, Levine JP, Gurtner GC. Quantitative and reproducible murine model of excisional wound healing. Wound Repair Regen 2004;12:485–492

23. Chen L, Tredget EE, Wu PY, Wu Y. Paracrine factors of mesenchymal stem cells recruit macrophages and endothelial lineage cells and enhance wound healing. PLoS One 2008;3:e1886

24. Rennert RC, Sorkin M, Januszyk M, et al. Diabetes impairs the angiogenic potential of adipose-derived stem cells by selectively depleting cellular subpopulations. Stem Cell Res Ther 2014;5:79

25. Yan J, Tie G, Wang S, et al. Type 2 diabetes restricts multipotency of mesenchymal stem cells and impairs their capacity to augment postischemic neovascularization in db/db mice. J Am Heart Assoc 2012;1:e002238

26. Singh B, Chatterjee A, Ronghe AM, Bhat NK, Bhat HK. Antioxidant-mediated up-regulation of OGG1 via NRF2 induction is associated with inhibition of oxidative DNA damage in estrogen-induced breast cancer. BMC Cancer 2013;13:253
27. Wu KC, Cui JY, Klaassen CD. Beneficial role of Nrf2 in regulating NADPH generation and consumption. Toxicol Sci 2011;123:590–600
28. Smith J, Ladi E, Mayer-Proschel M, Noble M. Redox state is a central modulator of the balance between self-renewal and differentiation in a dividing glial precursor cell. Proc Natl Acad Sci U S A 2000;97:10032–10037
29. Jang YY, Sharkis SJ. A low level of reactive oxygen species selects for primitive hematopoietic stem cells that may reside in the low-oxygenic niche. Blood 2007;110:3056–3063
30. Owusu-Ansah E, Banerjee U. Reactive oxygen species prime *Drosophila* haematopoietic progenitors for differentiation. Nature 2009;461:537–541
31. Tsai JJ, Dudakov JA, Takahashi K, et al. Nrf2 regulates haematopoietic stem cell function. Nat Cell Biol 2013;15:309–316
32. Hochmuth CE, Biteau B, Bohmann D, Jasper H. Redox regulation by Keap1 and Nrf2 controls intestinal stem cell proliferation in *Drosophila*. Cell Stem Cell 2011;8:188–199
33. Go MJ, Takenaka C, Ohgushi H. Forced expression of Sox2 or Nanog in human bone marrow derived mesenchymal stem cells maintains their expansion and differentiation capabilities. Exp Cell Res 2008;314:1147–1154
34. Zhu J, Wang H, Sun Q, et al. Nrf2 is required to maintain the self-renewal of glioma stem cells. BMC Cancer 2013;13:380
35. Yoon DS, Choi Y, Jang Y, et al. SIRT1 directly regulates SOX2 to maintain self-renewaland multipotency in bone marrow-derived mesenchymal stem cells. Stem Cells 2014;32:3219–3231
36. Pereira SL, Rodrigues AS, Sousa MI, Correia M, Perestrelo T, Ramalho-Santos J. From gametogenesis and stem cells to cancer: common metabolic themes. Hum Reprod Update 2014;20:924–943
37. Tormos KV, Anso E, Hamanaka RB, et al. Mitochondrial complex III ROS regulate adipocyte differentiation. Cell Metab 2011;14:537–544
38. Yates MS, Tran QT, Dolan PM, et al. Genetic versus chemoprotective activation of Nrf2 signaling: overlapping yet distinct gene expression profiles between Keap1 knockout and triterpenoid-treated mice. Carcinogenesis 2009;30:1024–1031
39. Januszyk M, Sorkin M, Glotzbach JP, et al. Diabetes irreversibly depletes bone marrow-derived mesenchymal progenitor cell subpopulations. Diabetes 2014;63:3047–3056